JACS
JOURNAL OF THE AMERICAN CHEMICAL SOCIETY
Article
pubs.acs.org/JACS

Measurement of State-Specific Association Constants in Allosteric Sensors through Molecular Stapling and NMR

Kody J. Moleschi,[†] Madoka Akimoto,[†] and Giuseppe Melacini*[,†,‡]

[†]Department of Chemistry and Chemical Biology, and [‡]Department of Biochemistry and Biomedical Sciences, McMaster University, 1280 Main Street West, Hamilton, Ontario L8S 4M1, Canada

Supporting Information

ABSTRACT: Allostery is a ubiquitous mechanism to control biological function and arises from the coupling of inhibitory and binding equilibria. The extent of coupling reflects the inactive vs active state selectivity of the allosteric effector. Hence, dissecting allosteric determinants requires quantification of state-specific association constants. However, observed association constants are typically population-averages, reporting on overall affinities but not on allosteric coupling. Here we propose a general method to measure state-specific association constants in allosteric sensors based on three key elements, i.e., state-selective molecular stapling through disulfide bridges, competition binding saturation transfer experiments and chemical shift correlation analyses to gauge state populations. The proposed approach was applied to the prototypical cyclic adenosine monophosphate (cAMP)-dependent protein kinase (PKA-RIα), for which the structures of the inactive and active states are available, as needed to design the state-selective disulfide bridges. Surprisingly, the PKA-RIα state-specific association constants are comparable to those of a structurally homologous domain with ~10^3-fold lower cAMP-affinity, suggesting that the affinity difference arises primarily from changes in the position of the dynamic apo inhibitory equilibrium.

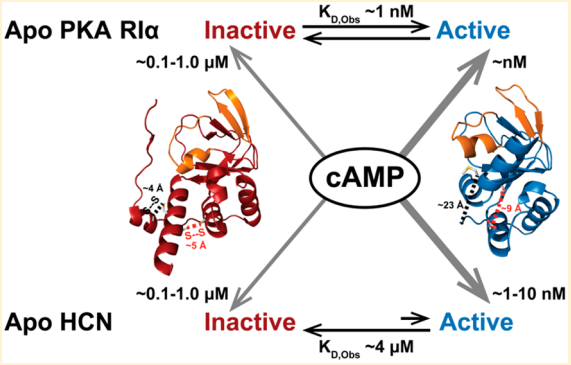

INTRODUCTION

Allosteric regulation is a fundamental control mechanism of biological systems,[1−23] and it has opened new opportunities to design antagonists and agonists with enhanced potency and selectivity for therapeutic targets previously considered undruggable.[24−28] A simple, but effective model to understand allostery elicited by a generic ligand relies on the four-state thermodynamic cycle arising from the coupling of two equilibria: the inhibitory (i.e., inactive vs active) equilibrium and the ligand-binding (i.e., apo vs holo) equilibrium (Figure 1a).[3,29−34] If the ligand does not exhibit active vs inactive selectivity, the binding and inhibitory equilibria are not coupled and binding occurs without activation or further inhibition (i.e., antagonism). If the ligand exhibits active vs inactive selectivity, ligand binding stabilizes the state with the highest affinity, leading to an allosteric conformational change (i.e., agonism or reverse-agonism). In general, the binding and inhibitory equilibria are allosterically coupled with a coupling free energy equivalent to

$$\Delta G_{\text{AllostericCoupling}} = RT \ln\left(\frac{K_{\text{a,Inactive}}}{K_{\text{a,Active}}}\right) \quad (1)$$

where $K_{\text{a,Inactive}}$ and $K_{\text{a,Active}}$ denote the association constants of the ligand for the inactive and active states of the allosteric protein, respectively. For agonists $K_{\text{a,Inactive}} < K_{\text{a,Active}}$, while for reverse-agonists $K_{\text{a,Inactive}} > K_{\text{a,Active}}$. Hence, measurements of state-specific association constants are essential for dissecting the driving forces underlying allosteric agonism and antagonism. However, currently available methods to measure affinities[35] focus primarily on the quantification of ensemble average association constants only. The observed average affinities are easily computed through binding polynomials (Supporting Information) based on the allosteric cycle of Figure 1a, showing that

$$K_{\text{a,Observed}} = X_{\text{Inactive,Apo}} K_{\text{a,Inactive}} + X_{\text{Active,Apo}} K_{\text{a,Active}} \quad (2)$$

where $X_{\text{Inactive,Apo}}$ and $X_{\text{Active,Apo}}$ denote the fractions of inactive and active states, respectively, in the absence of ligand. Eq 2 illustrates how the observed average affinities depend on both the position of the apo inhibitory equilibrium and the state-specific association constants. Even when the former is known, measurement of $K_{\text{a,Observed}}$ is not sufficient to determine the latter.

Here, we propose a general experimental approach to determine state-specific association constants. This can be achieved through traditional affinity measurements if the apo form of the allosteric system is trapped in either the pure inactive or active states. In principle, an efficient trapping

Received: June 30, 2015
Published: August 6, 2015

DOI: 10.1021/jacs.5b06557
J. Am. Chem. Soc. 2015, 137, 10777−10785

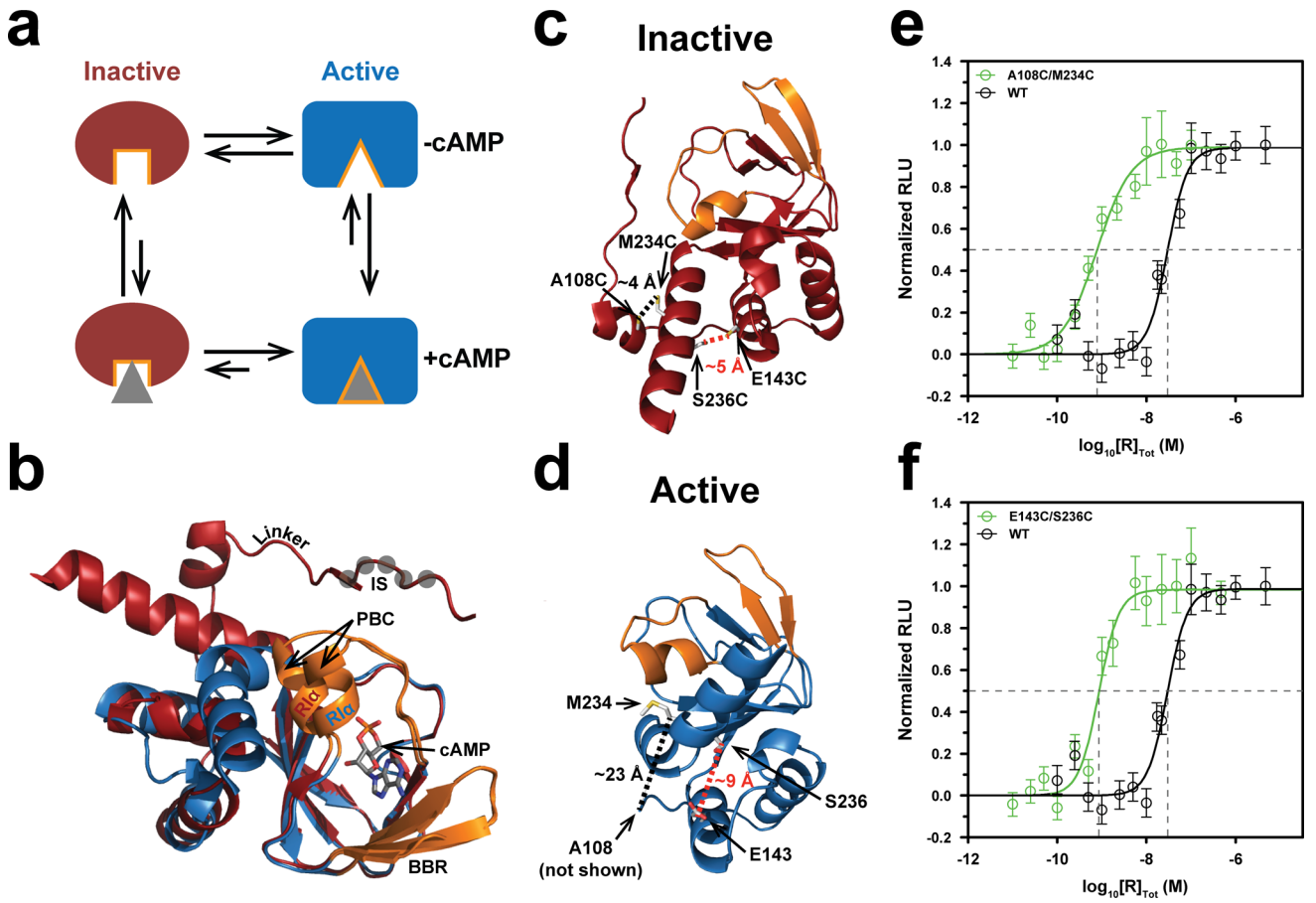

Figure 1. Allosteric thermodynamic cycle and state-selective trapping through molecular staples in PKA-RIα. (a) Apo RIα (91−244) samples both the active (blue) and inactive (red) states. The catalytic subunit of PKA preferentially binds the inactive state, while cAMP (gray) exhibits higher affinity for the active state. Weak cross-state interactions do exist, but little information is available due to the inherent dynamics of RIα. The cAMP binding pocket is shown in orange. (b) Overlay of the inactive (PDB: 2QCS) and active (PDB: 1RGS) structures. Color codes are as in panel (a). Gray circles indicate the residues in the kinase inhibitory site. (c,d) Design of molecular staples to stabilize the inactive state of RIα (91−244). The A108/M234 and E143/S236 residue pairs were mutated to cysteine for the purpose of disulfide bridge formation and stabilization of the inactive state. (e) Luminescence monitored kinase inhibition assay for A108C/M234C. Increasing amounts of RIα (91−244) were added to the PKA C-subunit to silence its catalytic activity. Increasing relative luminescence units (RLU) indicate enhanced inhibition. Significantly less disulfide-bridged RIα (green, IC_{50} = 0.8 nM) was required to inhibit C, as compared to WT RIα (black, IC_{50} = 29 nM). Error bars represent standard deviations of measurements performed in triplicate. (f) Same as (e), but for the E143C/S236C (green, IC_{50} = 0.9 nM).

method is provided by state-specific disulfide bridges, referred to here as "molecular staples". However, in practice, disulfide bridges alone rarely result in the isolation of pure states. Often molecular stapling simply provides a conformational bias toward the inactive or active states. Nevertheless, we show that the conformational bias provided by molecular stapling is sufficient to determine state-specific association constants, if it is combined with (a) measurements of the positions of the perturbed inhibitory equilibria based on NMR chemical shifts and with (b) competition binding experiments monitored by saturation transfer difference (STD) NMR spectra. When linear patterns of peak positions are observed in the disulfide-stapled mutants, the combination of conformational stapling through disulfide bridges, NMR chemical shift analyses, and competitive STD experiments results in a general approach for the measurement of state-specific association constants in allosteric regulators.

The proposed method to measure state-specific association constants is illustrated through its application to the regulatory subunit of the cyclic adenosine monophosphate (cAMP)-dependent protein kinase A (PKA-RIα), which represents a prototypical allosteric signaling system.[36−41] The central controlling unit of PKA-RIα comprises the (91−244) region, which includes the kinase inhibitory site and a single cAMP-binding domain (CBD) as well as the linker connecting them (Figure 1b).[42] RIα (91−244) fully inhibits the PKA catalytic subunit (C) in a cAMP-dependent manner and binds both cAMP and C with affinities comparable to full length RIα.[40,43] Although cAMP-binding to RIα (91−244) is slow in the NMR chemical shift time scale (at 700 MHz), the inactive vs active exchange is fast in both apo and holo forms,[36,40] and therefore measurement of state-specific affinities would be challenging without modification of RIα (91−244). Our results show that the state-specific association constants measured for RIα (91−244) using molecular stapling and NMR are comparable to those measured for another eukaryotic CBD, which binds cAMP with an affinity ~3 orders of magnitude weaker than that of RIα (91−244). The surprising similarity in state-specific association constants between these two CBDs suggests that the marked difference in their overall affinities arises primarily from changes in the position of the respective apo inhibitory equilibria.

DOI: 10.1021/jacs.5b06557
J. Am. Chem. Soc. 2015, 137, 10777−10785

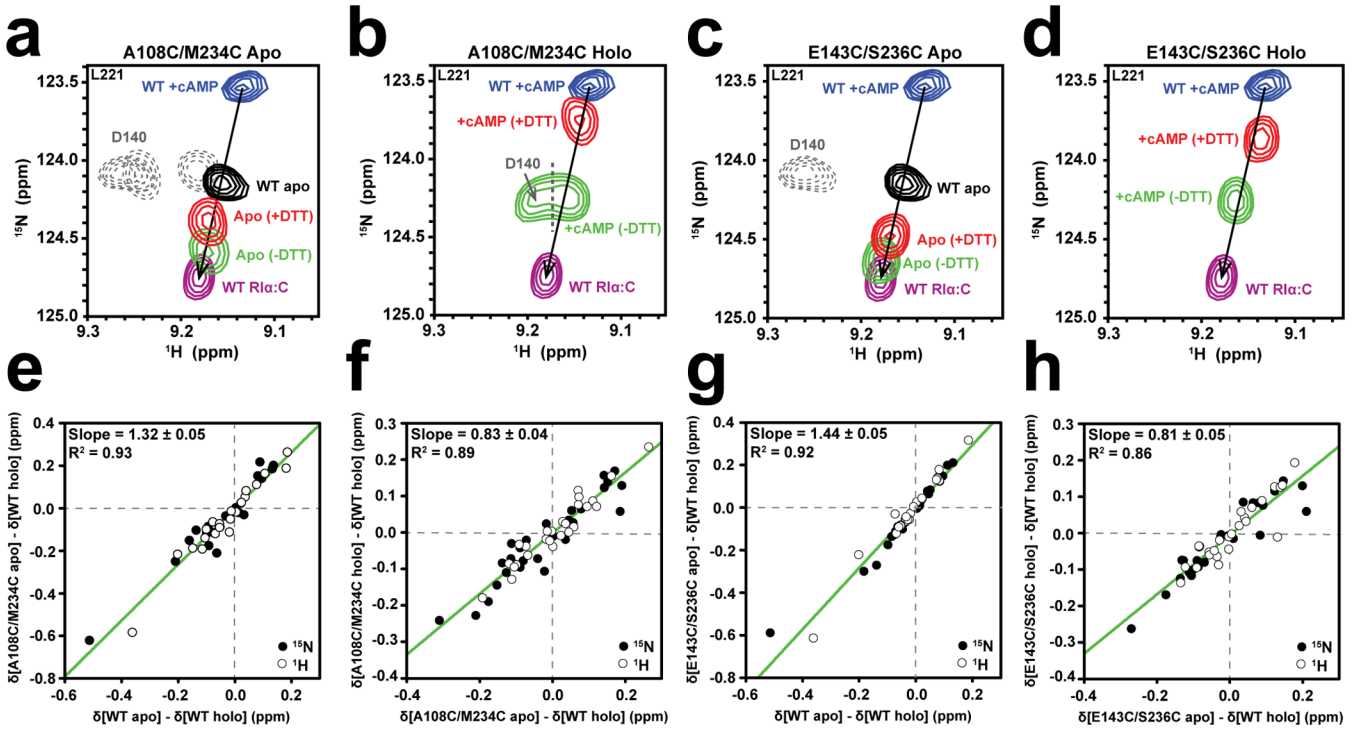

Figure 2. State-selective disulfide bridges partially stabilize the inactive state in both apo and holo forms. (a–d) Overlaid HSQC cross-peaks of reporter residue L221 for the disulfide mutants A108C/M234C and E143C/S236C RIα (91–244) in the absence (a,c) or presence (b,d) of cAMP. Because of fast exchange, the observed chemical shifts are linear averages and depend on the relative populations of the inactive and active states. (a) Apo A108C/M234C in the absence of DTT (green) exhibits greater inactive state population than WT apo. In the presence of DTT (red), the disulfide bridge is at least partially reduced, causing partial reversion toward WT apo by decreasing the proportion of the inactive state. (b) Similar to panel (a) but in the presence of excess cAMP. The cAMP-bound A108C/M234C disulfide bridged construct (green) preserves a significant population of inactivate state. (c) As (a), but for apo E143C/S236C. (d) As (c), but for cAMP-bound E143C/S236C. (e,f) Chemical shift correlation plots to measure the change in the overall extent of inactivation in the apo and holo disulfide-bridged A108C/M234C double mutant. Residues included in these plots were selected according to conditions (a–c) in p. S4 of the Supporting Information. Open and closed circles denote ^{1}H and ^{15}N chemical shift values, respectively, the latter scaled by 0.181.[47] On the basis of eqs S17 and S14, the slopes of the plots in panels (e) and (f) report on the relative changes in the inactive state populations. (g,h) As (e,f), but for E143C/S236C RIα (91–244).

RESULTS

Design of State-Selective Molecular Staples. The structures of RIα (91–244) bound to either cAMP (i.e., active state) or C (i.e., inactive state) have been solved,[44−46] and based on these structures we identified potential residue pairs to be used as sites for double mutations to cysteine. Such residue pairs meet two key conditions: (i) they are not part of the binding sites for the allosteric ligand to avoid affecting its affinity; (ii) they are close in the state to be stabilized by the disulfide bridge (e.g., Cβ–Cβ < 6 Å), but farther apart in the other (e.g., Cβ–Cβ > 8 Å). Two residue pairs that meet these criteria in RIα (91–244) are A108/M234 and E143/S236 (Figure 1c,d). These residue pairs are distal from the sites in contact with cAMP, i.e., the phosphate binding cassette and the base binding region (Figure 1c,d) and correspond to short distances in the inactive (e.g., Cβ–Cβ < 6 Å), but not in the active state (Figure 1c,d), suggesting that disulfide bridges at these locations should stabilize the inactive state. Hence, the two double cysteine mutants A108C/M234C and E143C/S236C were engineered and the resulting disulfide bridged constructs were assessed for their shifts in inhibitory equilibrium using a combination of kinase assays and NMR chemical shift analyses.

The Designed Disulfide Mutants Partially Stabilize the Inactive State of the Apo Form. For both A108C/M234C and E143C/S236C double mutants of PKA-RIα (91–244), kinase inhibition assays were performed in which luminescence measurements report on the amount of residual ATP. Higher luminescence values indicate higher concentrations of ATP and thus lower activities of the catalytic subunit of PKA (PKA-C), as shown in Figure 1e,f. Figure 1e,f illustrate that both disulfide mutants of RIα (91–244) inhibit PKA-C more effectively than wild type (WT) RIα (91–244). The IC_{50} values for A108C/M234C (0.8 nM) and E143C/S236C (0.9 nM) are similar, and at least 1 order of magnitude lower than that of WT (29 nM). The decreased IC_{50} values in the mutants vs WT confirm that the designed disulfide bridges successfully increase the fraction of inactive-state conformations, which exhibit high affinity for the catalytic subunit of PKA.

In order to quantify the increase in the inactive population resulting from the disulfide bridges, we took advantage of recently proposed NMR methods based on chemical shift projection and correlation analyses.[47−49] For this purpose, heteronuclear single quantum coherence (HSQC) spectra were collected for A108C/M234C and E143C/S236C RIα (91–244) both in the absence of cAMP and in the presence of saturating cAMP concentrations and compared to similar reference spectra acquired for WT RIα (91–244) in the apo, cAMP- and C-bound forms (Figure 2a–d). The apo, cAMP- and C-bound HSQC WT peak positions of residues that are sufficiently removed from both cAMP- and C-binding interfaces (e.g., L221) define linear patterns (Figure 2a–d), indicating

DOI: 10.1021/jacs.5b06557
J. Am. Chem. Soc. 2015, 137, 10777–10785

that such residues report primarily on the fast-exchanging active vs inactive equilibrium. Because of the population-weighted averaging occurring in the fast exchange regime, the active vs inactive fractions are encoded directly in the measured NMR chemical shifts. For instance, the WT apo peak is approximately equidistant from the WT RIα:cAMP and WT RIα:C peaks (Figure 2a), indicating that in WT apo the populations of the active and inactive states are similar, as determined previously.[40] However, for the A108C/M234C disulfide bridged mutant the apo peak (green) is shifted toward the WT RIα:C (purple) position (Figure 2a), pointing to an increase in the inactive state population relative to WT.

As a negative control to confirm that the increase in inactive state population is caused by the 108/234 disulfide bridge, HSQC spectra for the A108C/M234C mutant were also acquired in the presence of the reducing agent dithiothreitol (DTT) (red, Figure 2a). If inactive state immobilization relies on the molecular staple, it is expected that the spectra of the disulfide bridge mutants would be DTT dependent. When DTT is added to the sample, a partial reversion toward WT apo is observed (Figure 2a). It is possible that full reversion to WT apo is not observed because the reduced cysteine residues slightly perturb the inactive vs active equilibrium even prior to disulfide bridge formation and/or partial reoxidation occurs before data acquisition. In either case, the lack of full reversion to WT does not affect the measurement of state-specific association constants and Figure 2a clearly shows that the 108/234 disulfide bridge is effective in selectively stabilizing the inactive state of apo RIα (91−244), as sensed by the selected L221 reporter residue. In order to evaluate to what extent the 108/234 disulfide bridge perturbs the inhibitory equilibrium of cAMP-bound RIα (91−244), similar experiments were repeated in the presence of excess cAMP (Figure 2b).

The Designed Disulfide Mutants Partially Stabilize the Inactive State Even in the Holo Form. Figure 2b shows that the 108/234 disulfide bridge is effective in selectively stabilizing the inactive conformation over that of the active state of RIα (91−244), even in the presence of the endogenous allosteric activator, cAMP. As expected based on the disulfide bridge design criteria, under reducing conditions, the selective stabilization of the inactive state is markedly reduced (red, Figure 2b). Similar results are obtained for the L221 reporter residue of the other independent mutant E143C/S236C in both apo and cAMP-bound forms (Figure 2c,d). In order to prove that the inactive vs active state stabilization imparted by the disulfide bridges is not dependent on the specific choice of L221 as a reporter residue for the inhibitory equilibrium (Figure 2a−d), we measured the changes in the fractions of inactive state also by NMR chemical shift (δ) correlation analyses (Figure 2e,g).

Figure 2e,g shows the plot of ($\delta_{Mutant,Apo} - \delta_{WT,Holo}$) vs ($\delta_{WT,Apo} - \delta_{WT,Holo}$). This plot is expected to be linear with a slope equal to ($X_{Inactive,Mutant\ Apo}/X_{Inactive,WT\ Apo}$), i.e., the ratio between the fractions of inactive state in the mutant apo vs WT apo, provided it is restricted to residues that sense primarily the position of the inhibitory equilibrium (Supporting Information: residue selection criteria (a−c) p. S4 and eq S17). The resulting plot for the apo A108C/M234C mutant is shown in Figure 2e providing a ($X_{Inactive,Mutant\ Apo}/X_{Inactive,WT\ Apo}$) ratio of 1.32 ± 0.05; i.e., the 108/234 disulfide bridge leads to an overall ∼30% increase in the apo inactive population.

A similar approach was utilized to quantify the change in inactive fraction of the holo form. The plot of ($\delta_{Mutant,Holo} - \delta_{WT,Holo}$) vs ($\delta_{Mutant,Apo} - \delta_{WT,Holo}$) for residues reporting on the inhibitory equilibrium is expected to be linear with a slope equal to the ($X_{Inactive,Mutant\ Holo}/X_{Inactive,Mutant\ Apo}$) ratio (Supporting Information: eq S14), which in the case of the A108C/M234C mutant is 0.83 ± 0.04 (Figure 2f). This result means that unlike WT, the 108/234 disulfide mutant limits the decrease in the inactive fraction upon cAMP saturation to just ∼15%. Similar results were obtained for the E143C/S236C mutant (Figure 2g,h). Overall, the data of Figure 2 clearly indicate that each independent disulfide bridge successfully shifts the inhibitory equilibrium of RIα (91−244) toward the inactive state in both apo and cAMP-bound forms, but residual populations of active state remain in both forms of the disulfide bridged mutants. Given the higher-affinity of cAMP for the active vs inactive state, it is essential to account for the presence of residual active state populations when using the disulfide bridges as molecular staples for determining the association constant of the inactive state. This approach is preferred to other methods introducing additional, potentially invasive perturbations to further stabilize the inactive conformation.

Accounting for Residual Active State Populations. The effect of the residual active state population in the disulfide-bridged mutants designed to trap the inactive state is corrected through the following equation (Supporting Information):

$$K_{a,Inactive} = K_{a,Observed}\frac{X_{Inactive,Holo}}{X_{Inactive,Apo}} \quad (3)$$

where $X_{Inactive,Holo}$ denotes the fraction of inactive state in the presence of saturating amounts of ligand (i.e., large cAMP excess) and the other terms are defined as in eq 2. In principle eq 3 applies to both WT and mutant proteins, however in the case of WT, the $X_{Inactive,Holo}$ term is often minimal (∼0%) and typically affected by a high relative error. Because of the challenges in accurately determining $X_{Inactive,WT\ Holo}$, eq 3 is of little practical utility for the WT protein. However, when eq 3 is applied to the disulfide mutants designed to stabilize the inactive state, $X_{Inactive,Mutant\ Holo}$ is significantly higher than 0% (e.g., >50% based on Figure 2b,d,f,h) and is determined more accurately, making eq 3 an excellent tool to determine state-specific association constants. It should be noted that eq 3 was derived for the inactive state as this is the state stabilized by the designed molecular staples used here, but a similar equation applies for the active state as well (Supporting Information: eq S9), and it is useful when the molecular staples selectively stabilize the active state. The implementation of eq 3 requires the determination of $K_{a,Observed}$ and of the ($X_{Inactive,Holo}/X_{Inactive,Apo}$) ratio for the mutants. The latter is measured directly through the slope of the ($\delta_{Mutant,Holo} - \delta_{WT,Holo}$) vs ($\delta_{Mutant,Apo} - \delta_{WT,Holo}$) plots shown in Figure 2f,h. Hence, the last measurement needed to obtain $K_{Inactive}$ from eq 3 is that of $K_{a,Observed}$.

Measurement of $K_{a,Observed}$ for the Disulfide Mutants. Saturation transfer difference (STD) NMR spectroscopy is a robust label-free method to quantify affinities, but the STD signal is typically weak for tightly bound complexes (K_D < ∼μM).[50] This was the case for cAMP binding to the disulfide mutants due to the presence of residual populations of active state, which exhibits high affinity for cAMP and leads to a marginal STD signal for cAMP (Supporting Figure S3). To circumvent this problem and widen the K_D window of applicability of the STD measurement, competition-binding

DOI: 10.1021/jacs.5b06557
J. Am. Chem. Soc. 2015, 137, 10777−10785

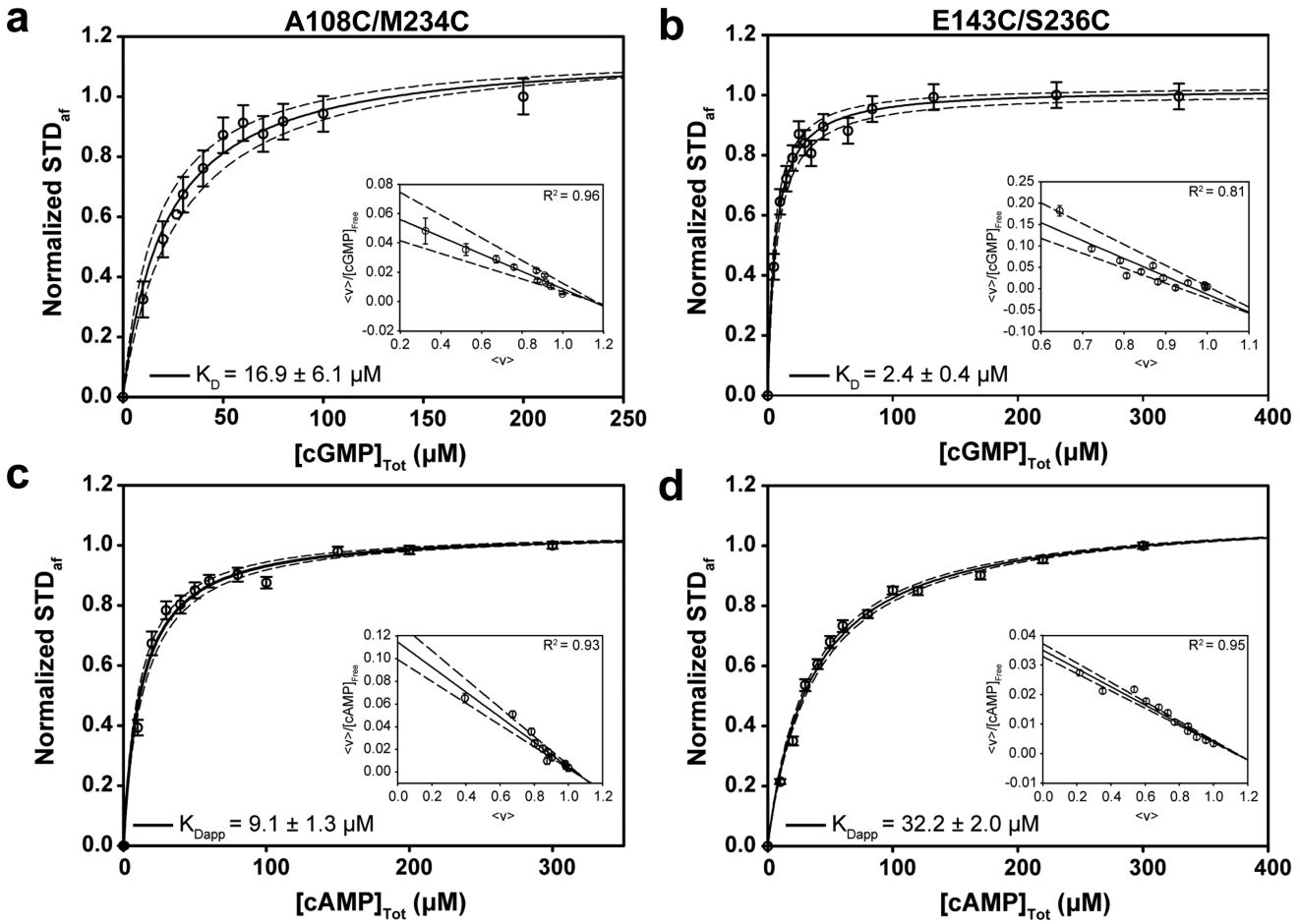

Figure 3. Measuring affinities for the "stapled" mutants. (a) Isotherm for the binding of cGMP to the A108C/M234C disulfide-bridged mutant of RIα (91−244). The dissociation constant of cGMP is required to determine the $K_{D,Obs}$ of cAMP from the competition experiment. The STD/STR ratio from the ribose H1′ was used to build the dose−response curve. Inset: Scatchard plot ($\langle v\rangle/[L]$ vs $\langle v\rangle$) used to calculate the dissociation constant ($K_{D,cGMP}$ = 16.9 ± 6.1 μM). Dashed curves were obtained using the "edge" values of K_D (e.g., 10.8 and 23.0 μM). (b) As (a), but for the E143C/S236C double mutant ($K_{D,cGMP}$ = 2.4 ± 0.4 μM). (c) Binding isotherm for the cAMP-titration of A108C/M234C presaturated with 500 μM cGMP ($K_{Dapp,cAMP}$ = 9.1 ± 1.3 μM). (d) As (c), except for the disulfide mutant E143C/S236C ($K_{Dapp,cAMP}$ = 32.2 ± 2.0 μM).

Table 1. Summary of Observed and State-Specific K_D Values

cAMP-binding domain (CBD)	cGMP K_D (μM)	cAMP K_{Dapp} (μM)	cAMP $K_{D,Obs}$ (μM)[a]	$(X_{In,Holo}/X_{In,Apo})$	cAMP $K_{D,In}$ (μM)	cAMP $K_{D,Ac}$ (μM)
A108C/M234C RIα (91−244)	16.9 ± 6.1	9.1 ± 1.3	0.30 ± 0.10	0.83 ± 0.04	0.36 ± 0.12	–
E143C/S236C RIα (91−244)	2.4 ± 0.4	32.2 ± 2.0	0.16 ± 0.03	0.81 ± 0.05	0.20 ± 0.04	–
WT RIα (91−244)	–	–	$(1.0 \pm 0.1)10^{-3}$[a]	–	0.28 ± 0.06[b]	$(0.5 \pm 0.1)10^{-3}$
WT HCN2	–	–	3.6 ± 1.3[c]	–	0.84[d]	$(8.0)10^{-3}$[d]

[a]From ref 40. [b]Average $K_{D,Inactive}$ between disulfide mutants. [c]From ref 54. [d]From ref 52.

experiments were performed with cyclic guanosine monophosphate (cGMP). cGMP binds PKA-RIα at the same site as cAMP but more weakly, resulting in a detectable STD signal for cGMP (Supporting Figure S3). This is because the addition of the cGMP amino group at position C2 of the guanine base clashes with the phosphate binding cassette, thereby exhibiting lower affinity.[39] Furthermore, several ^{1}H NMR signals of cGMP are well resolved from those of cAMP (e.g., ^{1}H1′, Supporting Figure S3). Because of these properties, in the presence of cGMP it is possible to measure an STD signal for cAMP, which is utilized to monitor the competitive binding of cAMP to a mutant sample preloaded with an excess of cGMP, as shown in Figure 3c,d. The apparent K_D ($K_{Dapp,Obs}$) obtained from the cAMP vs cGMP competitive binding experiment (Figure 3c,d) is then scaled down to the actual $K_{D,Obs}$ for cAMP using Supporting eq S18 (Supporting Information) and the STD-derived K_D for cGMP (Figure 3a,b).

Determining the State-Specific Association Constants. The resulting K_D for cGMP as well as the $K_{D,apparent}$ and $K_{D,Observed}$ for cAMP binding to both disulfide mutants are summarized in Table 1. The observed cAMP K_D values for A108C/M234C and E143C/S236C are 0.30 ± 0.1 μM and 0.16 ± 0.03 μM, respectively (Table 1). However, these observed dissociation constants are not the inactive-state specific K_D values, as they must first be corrected for the holo/apo inactive populations according to eq 3. Using the $(X_{Inactive,Holo}/X_{Inactive,Apo})$ ratios from the slope of the chemical shift plots (Figure 2f,h) to scale down according to eq 3 the $K_{D,Observed}$ from the STD competition experiments, the inactive-state specific K_D values are obtained, i.e., $K_{D,Inactive}$ = 0.36 ± 0.12

DOI: 10.1021/jacs.5b06557
J. Am. Chem. Soc. 2015, 137, 10777−10785

μM and 0.20 ± 0.04 μM for A108C/M234C and E143C/S236C, respectively (Table 1). Although these two dissociation constants were measured for two independent and distinct inactive-state trapping disulfide mutants, their difference is not significant, corroborating the robustness of the proposed approach and suggesting that the values obtained from the two disulfide bridges can be combined into a single average inactive-state specific K_D (i.e., $1/K_{a,Inactive}$) value of 0.28 ± 0.06 μM for PKA-RIα (91−244) (Table 1).

Once the $K_{a,Inactive}$ is determined, the active-state specific K_a (i.e., $K_{a,Active}$) is obtained through eq 2 using the known $K_{a,Observed}$ and the inactive vs active molar fractions measured for apo WT.[40] The resulting $K_{D,Active}$ value (i.e., 0.5 ± 0.1 nM, Table 1) is ∼ three-orders of magnitude lower than the $K_{D,Inactive}$. Since $K_{a,Active} \gg K_{a,Inactive}$, the $K_{a,Active}$ term in eq 2 dominates the average, demonstrating that it would have been challenging to determine the $K_{a,Inactive}$ without the aid of inactive-state selective molecular staples (e.g., disulfide bridges).

DISCUSSION

Using the proposed protocol, which combines molecular stapling with both ligand- and protein-based NMR as summarized in Figure 5, we have determined that the $K_{D,Inactive}$ and $K_{D,Active}$ state-specific dissociation constants for the PKA-RIα (91−244):cAMP complex are in the sub-μM and ∼nM ranges, respectively (Table 1). These values correspond to a ΔG of allosteric coupling of ∼−6 RT (eq 1), which is sufficient to reach active state populations >90% when RIα is cAMP-bound.[40] Furthermore, the sub-μM and ∼nM ranges for the $K_{D,Inactive}$ and $K_{D,Active}$ state-specific dissociation constants of PKA-RIα (91−244) compare well with those independently measured for a structurally homologous domain, i.e., the CBD of the hyperpolarization and cyclic-nucleotide gated (HCN) ion channels (Table 1).[51,52] Unlike other cAMP-regulated signaling systems, the open vs closed states of the HCN channel can be selectively stabilized independently of cAMP by voltage alone and therefore the open vs closed dissociation constants are accessible through patch clamp electrophysiology.[51] To the extent that the open/closed states of the HCN channel represent the active/inactive states of the HCN CBD, the currently available active and inactive dissociations constants for the CBD of HCN2 fall in the sub-μM and nM range,[51,52] respectively, similarly to those independently measured here for PKA-RIα (91−244) using molecular stapling (Table 1).

The similarity in state-specific association constants between the CBDs of HCN and PKA is remarkable because HCN and PKA bind cAMP with markedly different affinities. While HCN2 exhibits a μM affinity for cAMP, PKA-RIα binds cAMP with an observed K_D in the nM range.[40,53,54] Considering that the observed affinities are averages, as shown by eq 2, the similarity in the state-specific association constants between HCN and PKA implies that the ∼3-order of magnitude difference in cAMP affinities arises primarily from changes in the position of the apo inhibitory equilibrium (Figure 4). This prediction is confirmed by recent investigations showing that the HCN inactive vs active apo populations are significantly different, i.e., the apo HCN autoinhibitory equilibrium is highly skewed toward the inactive (low-affinity) state,[53] unlike apo PKA RIα (91−244) for which the inactive vs active populations are comparable (Figure 4).[40]

Overall, our measurements reveal that the CBD state-specific association constants are largely CBD-independent, suggesting

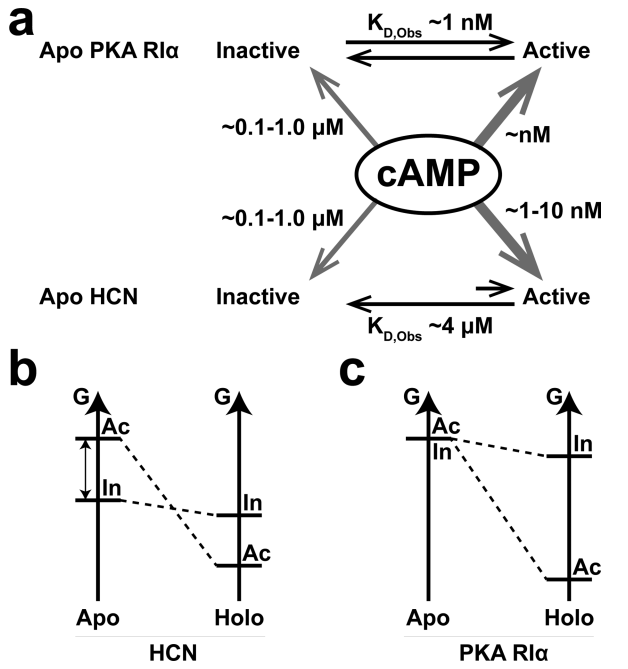

Figure 4. Apo population, state-specific K_D, and free energy comparison for RIα and HCN. (a) RIα and HCN bind cAMP with similar affinities when either in the active (∼nM) or inactive (∼sub-μM) conformations (thick gray arrows vs thin gray arrows), yet display a ∼10^3 difference in observed K_D. This is because their respective apo populations of active vs inactive states differ significantly (black arrows). Apo PKA-RIα samples active and inactive forms ∼ equally (∼50%), while apo HCN mainly exists in the inactive state, resulting in lower cAMP affinity. (b,c) Free energy differences between active (Ac) and inactive (In) states of the apo and cAMP-bound (holo) forms of HCN (b) and PKA-RIα (c). The free energy diagram illustrates qualitative changes and is not to scale.

the possibility that differences in cAMP-affinities between CBDs are to a large extent dictated by the dynamics of the apo CBDs rather than by the structures of the holo CBDs, which appear to be largely conserved across different eukaryotic CBDs.[55] While this principle was proven here only for two CBDs of HCN and PKA, it highlights the critical role of differential dynamics in determining binding selectivity.

The sub-μM value determined for $K_{D,Inactive}$ through the proposed molecular stapling approach (Table 1) is lower than the dissociation constant for cAMP binding to the C-bound RIα (91−244), which was previously determined to fall in the ∼3−100 μM range.[46,40,56] The reduced cAMP-affinity of the R:C complex compared to the inactive state of the *apo* R-subunit is explained by the direct contacts between the C-subunit of PKA and the phosphate binding cassette (PBC) of PKA-RIα (91−244), which in turn weaken the interactions between cAMP and the PBC.[57] These observations illustrate that a reliable measurement of state-specific association constants for PKA-R requires that the inactive state of PKA-R be selectively stabilized in the absence of PKA-C.

In conclusion, we have proposed and applied a general method to measure state-specific association constants of allosteric sensors based on three key elements, i.e., molecular stapling through disulfide bridges, competition binding STD experiments and chemical shift correlation analyses (Figure 5). The disulfide "staples" are designed to exploit active vs inactive structural differences and stabilize selected conformational states in both apo and holo forms. As it is often difficult to

DOI: 10.1021/jacs.5b06557
J. Am. Chem. Soc. 2015, 137, 10777−10785

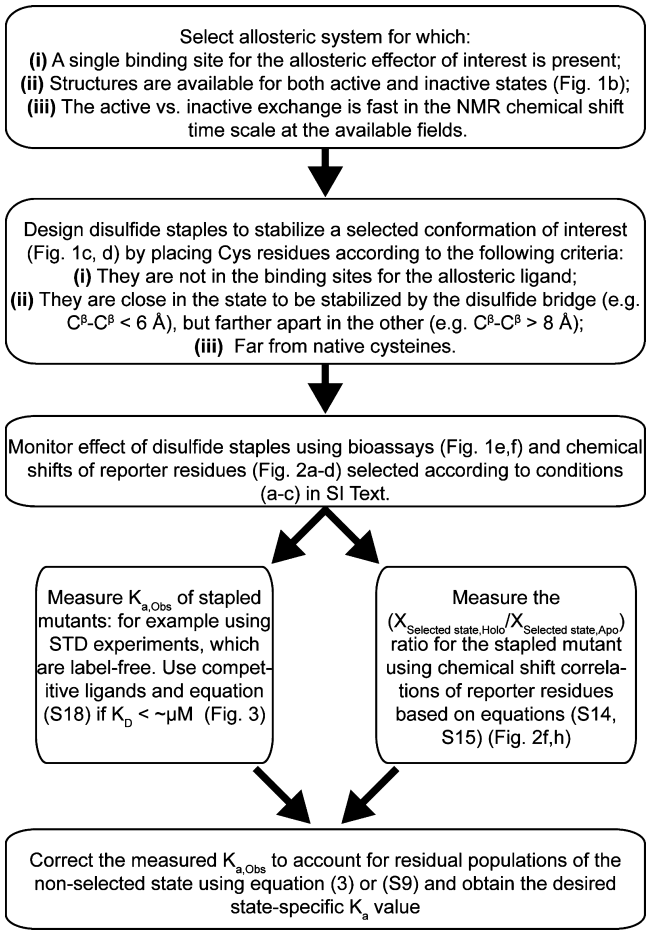

Figure 5. Summary flowchart of the protocol proposed to measure state-specific association constants in allosteric sensors. A similar flowchart is applicable also when the $K_{a,Obs}$ values are measured by methods different from STD (e.g., isothermal titration calorimetry, surface plasmon resonance, fluorescence based methods, etc.) or when the active vs inactive equilibrium is perturbed by modifications different from disulfide bridges (e.g., point mutations, post-translational modifications, etc.).

achieve full immobilization of the selected state, we also developed an approach to account for residual populations of alternative states through eq 3, which requires the measurements of both the mutant association constant and the state-specific populations. The former is effectively obtained through STD competition experiments, which provide a label-free access to a wide-window of association constants and are applicable to large MW systems. The latter are derived from chemical shift correlation and projection analyses.[47,49] Eq 3 is applied to different "stapled" mutants, which serve as reciprocal controls and provide multiple determinations of state-specific association constants. The convergence of these independent measurements to a consensus set of state-specific association constants supports the noninvasive nature of the designed molecular staples.

While the proposed approach was illustrated here for PKA-RIα, the method is general and transferrable to other allosteric sensors, offering otherwise elusive insight on the determinants of binding affinities and of allosteric coupling (i.e., eqs 1 and 2). For example, through the approach outlined here (Figure 5) it was possible to address a long outstanding question about the ~3-order of magnitude higher affinity of PKA-RIα relative to other structurally homologous cAMP-binding domains (e.g., HCN). This apparent paradox was solved by showing that the state-specific association constants of the cAMP-binding domains of PKA-RIα and HCN are surprisingly similar, but the positions of their apo dynamic inhibitory equilibria are markedly different. These observations clearly illustrate that the dynamics of the apo forms is a critical determinant of affinities. Furthermore, the measurement of $K_{a,Inactive}$ provides a first level of characterization of the holo-inactive intermediate state complex (Figure 1a), which is often only transiently populated but critical to facilitate the design of allosteric inhibitors.

MATERIALS AND METHODS

Expression and Purification of PKA-RIα (91−244). All mutations were generated using a variation of the Quikchange protocol. A pTRiEX plasmid encoding the small ubiquitin-like modifier/cAMP-dependent protein kinase (SUMO-PKA-RIα) fusion protein was expressed and purified as previously described.[40] To increase yields, the insoluble pellet fraction was recovered and resuspended in 8 M urea wash buffer, and subjected to Ni^{2+} affinity chromatography under denaturing conditions. The eluted protein was dialyzed to native conditions in the presence of TEV protease for simultaneous refolding and cleavage.

Disulfide State Trapping. The disulfide bridged proteins were kept reduced at every step of the preparation protocol until samples were ready for spectroscopic studies. Extensive dialysis (4 × 1 L for ~2 h followed by 1 × 4 L overnight at room temperature) was then utilized for buffer-exchange into the NMR buffer (50 mM MOPS pH 7, 100 mM NaCl, 10 mM $MgCl_2$, 0.02% NaN_3) and oxidation of the cysteines. It should be noted that no cysteines are native to PKA-RIα (91−244). Mutants were then concentrated with centrifugal filters (10 kDa MWCO, Millipore) to 100 μM and supplemented with 5% D_2O for locking purposes. In the case of reduced samples, 5 mM DTT was added and incubated for 1 h at room temperature. The mutant sample integrity was checked by both SEC chromatography (Superdex 75 or 200, GE) and NMR. No significant differences were observed between the elution volumes of the mutants and the WT in the absence of DTT, indicating that the cysteine mutations did not result in the formation of soluble aggregates. In addition, the NMR signal-to-noise ratios in the HSQC spectra of the mutants and WT were comparable further ruling out potential mutation-induced aggregates/oligomers.

Inhibition Kinase Assay. RIα (91−244) at different concentrations (10^{-2} nM − 4.68×10^3 nM) was incubated with the catalytic subunit (4 nM) at room temperature for 10 min in the assay buffer (40 mM Tris-HCl pH 7.5, 0.1 mg/mL BSA, and 20 mM $MgCl_2$), as previously described.[40] Two assay reagents, 10 μM Kemptide and 10 μM ATP, were then added to the assay buffer to reach a total volume of 50 μL and to start the phosphorylation reactions. Reactions were allowed to proceed for 60 min after which 50 μL of Ultra-Glo luciferase solution were added. Two controls were also prepared, consisting of a reaction with no Kemptide to provide the maximal luminescence, and another reaction with only RIα absent to obtain the minimal luminescence. Luminescence was measured with a TECAN infinite M200 plate reader.

PKA-RIα (91−244) Inactive State Population Assessment by NMR. Uniformly ^{15}N-labeled proteins at 100 μM were supplemented with both 5% D_2O for locking, and ^{15}N-acetyl−glycine for referencing. For the holo samples, cAMP was added at a total concentration of 1 mM. Sensitivity enhanced heteronuclear single quantum coherence (HSQC) spectra were acquired for all samples in apo and excess +cAMP forms, both with or without DTT, on a Bruker AV 700 spectrometer equipped with a TCI cryogenic probe. Spectra included 256 (t_1) and 1024 (t_2) complex points over spectral widths of 31.82 and 14.06 ppm for the ^{15}N and ^{1}H dimensions, respectively, and were recorded with 4 scans and a 1.70 s recycle delay. Carrier frequencies of ^{1}H and ^{15}N were set at the water and central amide region, respectively. All spectra were recorded at 306 K and processed using NMRpipe[58] with linear prediction. Spectra were analyzed utilizing

DOI: 10.1021/jacs.5b06557
J. Am. Chem. Soc. 2015, 137, 10777−10785

Sparky[59] and Gaussian line-fitting. Resonance assignments were established through spectral comparisons with WT RIα (91−244). The combined ^{15}N and ^{1}H chemical shifts were computed as

$$\Delta\delta = [(\Delta\delta_{1H})^2 + (0.2\Delta\delta_{15N})^2]^{1/2} \quad (4)$$

and a chemical shift cutoff of 0.05 ppm was implemented for the chemical shift projection analyses (CHESPA) (Supporting Information).[48,49] The apo and cAMP-bound wild-type forms served as the CHESPA reference states to evaluate the effect of the perturbed state, i.e., the apo or cAMP-bound mutant. The fractional activation and cos(θ) values were calculated as previously described.[49]

STD Experiments and Competition Binding Measurements. Purified RIα (91−244) mutants at a concentration of 10 μM were buffer exchanged into 20 mM NaH_2PO_4 pH 6.5, 50 mM NaCl in ≥99% D_2O using disposable PD-10 desalting columns (GE) or centrifugal Zeba filters (Thermo Scientific). Reference (STR) and difference (STD) ^{1}H spectra with water-gate water suppression were acquired for all samples at 298 K. Off-resonance saturation occurred at 30 ppm, while on-resonance irradiation was placed at 0.79 ppm. This ensured selective irradiation of the protein and not the ligand. A short spin-lock of 5 ms was applied to minimize protein signal interference, while also avoiding reduction in ligand signals. Spectra were digitized with 16 K complex points. The spectral width was 13.03 ppm centered at 4.71 ppm, with 1024 or 512 scans and 8 dummy scans for the STD experiments. For the more sensitive STR experiments, 128 scans were used.

Dissociation constants for the disulfide mutants with cGMP and cAMP were measured by quantifying the fraction of protein bound ($\langle\nu\rangle$) through the normalized STD amplification factor (STD_{af}) method.[50] Ligand concentrations varied between 10 μM to 320 μM. In the case of competition experiments, samples were presaturated with 500 μM cGMP, and then titrated with increasing amounts of cAMP. Upon addition of cAMP, the sample was incubated at room temperature for 30 min to ensure complete ligand equilibration prior to NMR data acquisition. STD_{af} was determined from the product of the STD:STR ratio, measured for the $^{1}H1'$ cAMP ribose, and the ratio of total ligand and protein concentration.[50] The STD_{af} values were normalized to the largest STD_{af} to obtain the fraction of protein bound ($\langle\nu\rangle$):

$$\langle\nu\rangle = \frac{STD_{af}}{STD_{af,max}} \quad (5)$$

The experimental $\langle\nu\rangle$ values were then modeled according to the 1:1 binding isotherm:

$$\langle\nu\rangle = \frac{[L]}{K_D + [L]} \quad (6)$$

where $[L]$ is the concentration of free cAMP or cGMP and K_D denotes either the K_{Dapp} for cAMP or the actual K_D for cGMP. $[L]$ was obtained from $[L]_{Total}$ by subtracting the concentration of bound ligand:

$$[L] = [L]_{Total} - (\langle\nu\rangle[P]_{Total}) \quad (7)$$

Both the cGMP K_D and the cAMP K_{Dapp} values were determined using Scatchard plots ($\langle\nu\rangle/[L]$ vs $\langle\nu\rangle$) by computing the negative reciprocal of the slope. The K_{Dapp} values for cAMP were converted to $K_{D,Obs}$ through the eq S18.

■ ASSOCIATED CONTENT

Supporting Information

The Supporting Information is available free of charge on the ACS Publications website at DOI: 10.1021/jacs.5b06557.

Derivations of eqs 2 and 3; measurement of population ratios through chemical shift correlations; analysis of competition binding experiments; Figures S1−S3. (PDF)

■ AUTHOR INFORMATION

Corresponding Author

*melacin@mcmaster.ca

Notes

The authors declare no competing financial interest.

■ ACKNOWLEDGMENTS

We thank S. Boulton, N. Jafari, Dr. S.S. Taylor, Dr. C.G. Kalodimos, Dr. A. Guarné and M. Gloyd for helpful discussion. This manuscript is dedicated to the memory of our friend and colleague, Dr. Veronica Esposito (1974−2013). This work was supported by grant (MOP-68897) from the Canadian Institutes of Health Research (CIHR) and grant (RGPIN-2014−04514) from the Natural Sciences and Engineering Research Council of Canada (NSERC).

■ REFERENCES

(1) Kuriyan, J.; Eisenberg, D. *Nature* **2007**, *450*, 983−990.
(2) Ruschak, a M.; Kay, L. E. *Proc. Natl. Acad. Sci. U. S. A.* **2012**, *109*, E3454−E3462.
(3) Vendruscolo, M. *Nat. Chem. Biol.* **2011**, *7*, 411−412.
(4) Changeux, J.-P.; Edelstein, S. J. *Science* **2005**, *308*, 1424−1428.
(5) Gardino, A. K.; Villali, J.; Kivenson, A.; Lei, M.; Liu, C. F.; Steindel, P.; Eisenmesser, E. Z.; Labeikovsky, W.; Wolf-Watz, M.; Clarkson, M. W.; Kern, D. *Cell* **2009**, *139*, 1109−1118.
(6) Kern, D.; Zuiderweg, E. R. P. *Curr. Opin. Struct. Biol.* **2003**, *13*, 748−757.
(7) Aghazadeh, B.; Lowry, W. E.; Huang, X. Y.; Rosen, M. K. *Cell* **2000**, *102*, 625−633.
(8) Long, D.; Brüschweiler, R. *J. Am. Chem. Soc.* **2011**, *133*, 18999−19005.
(9) Smock, R. G.; Gierasch, L. M. *Science* **2009**, *324*, 198−203.
(10) Tzeng, S.-R.; Kalodimos, C. G. *Nature* **2009**, *462*, 368−372.
(11) Boehr, D. D.; Nussinov, R.; Wright, P. E. *Nat. Chem. Biol.* **2009**, *5*, 789−796.
(12) Hayashi, I.; Wilde, A.; Mal, T. K.; Ikura, M. *Mol. Cell* **2005**, *19*, 449−460.
(13) Religa, T. L.; Sprangers, R.; Kay, L. E. *Science* **2010**, *328*, 98−102.
(14) Kim, J.; Masterson, L. R.; Cembran, A.; Verardi, R.; Shi, L.; Gao, J.; Taylor, S. S.; Veglia, G. *Proc. Natl. Acad. Sci. U. S. A.* **2015**, 201502299.
(15) Ishiyama, N.; Lee, S. H.; Liu, S.; Li, G. Y.; Smith, M. J.; Reichardt, L. F.; Ikura, M. *Cell* **2010**, *141*, 117−128.
(16) Whittier, S. K.; Hengge, A. C.; Loria, J. P. *Science* **2013**, *341*, 899−903.
(17) Masterson, L. R.; Yu, T.; Shi, L.; Wang, Y.; Gustavsson, M.; Mueller, M. M.; Veglia, G. *J. Mol. Biol.* **2011**, *412*, 155−164.
(18) Srivastava, A. K.; McDonald, L. R.; Cembran, A.; Kim, J.; Masterson, L. R.; McClendon, C. L.; Taylor, S. S.; Veglia, G. *Structure* **2014**, *22*, 1735−1743.
(19) VanSchouwen, B.; Akimoto, M.; Sayadi, M.; Fogolari, F.; Melacini, G. *J. Biol. Chem.* **2015**, *290*, 17642−54.
(20) Smith, M. J.; Ikura, M. *Nat. Chem. Biol.* **2014**, *10*, 223−230.
(21) Mazhab-Jafari, M. T.; Das, R.; Fotheringham, S. a.; SilDas, S.; Chowdhury, S.; Melacini, G. *J. Am. Chem. Soc.* **2007**, *129*, 14482−14492.
(22) Jayaraman, B.; Nicholson, L. K. *Biochemistry* **2007**, *46*, 12174−12189.
(23) Blyuss, K. B.; Nicholson, L. B. *J. Theor. Biol.* **2012**, *308*, 45−55.
(24) Courilleau, D.; Bisserier, M.; Jullian, J. C.; Lucas, A.; Bouyssou, P.; Fischmeister, R.; Blondeau, J. P.; Lezoualc'h, F. *J. Biol. Chem.* **2012**, *287*, 44192−44202.
(25) Courilleau, D.; Bouyssou, P.; Fischmeister, R.; Lezoualc'h, F.; Blondeau, J. P. *Biochem. Biophys. Res. Commun.* **2013**, *440*, 433−448.
(26) Nussinov, R.; Tsai, C. J. *Trends Pharmacol. Sci.* **2014**, *35*, 256−264.

DOI: 10.1021/jacs.5b06557
J. Am. Chem. Soc. 2015, 137, 10777−10785

(27) Tzeng, S.-R.; Kalodimos, C. G. *Nat. Chem. Biol.* **2013**, *9*, 462−465.
(28) Das, R.; Melacini, G. *J. Biol. Chem.* **2007**, *282*, 581−593.
(29) Nussinov, R.; Ma, B.; Tsai, C. J. *Biophys. Chem.* **2014**, *186*, 22−30.
(30) Tzeng, S.-R.; Kalodimos, C. G. *Nature* **2012**, *488*, 236−240.
(31) De, S.; Greenwood, A. I.; Rogals, M. J.; Kovrigin, E. L.; Lu, K. P.; Nicholson, L. K. *Biochemistry* **2012**, *51*, 8583−8596.
(32) Baldwin, A. J.; Kay, L. E. *Nature* **2012**, *488*, 165−166.
(33) Selvaratnam, R.; Chowdhury, S.; VanSchouwen, B.; Melacini, G. *Proc. Natl. Acad. Sci. U. S. A.* **2011**, *108*, 6133−6138.
(34) Boulton, S.; Akimoto, M.; Selvaratnam, R.; Bashiri, A.; Melacini, G. *Sci. Rep.* **2014**, *4*, 7306.
(35) Pollard, T. D. *Mol. Biol. Cell* **2010**, *21*, 4061−4067.
(36) Das, R.; Esposito, V.; Abu-Abed, M.; Anand, G. S.; Taylor, S. S.; Melacini, G. *Proc. Natl. Acad. Sci. U. S. A.* **2007**, *104*, 93−98.
(37) McNicholl, E. T.; Das, R.; SilDas, S.; Taylor, S. S.; Melacini, G. *J. Biol. Chem.* **2010**, *285*, 15523−15537.
(38) Sjoberg, T. J.; Kornev, A. P.; Taylor, S. S. *Protein Sci.* **2010**, *19*, 1213−1221.
(39) Das, R.; Chowdhury, S.; Mazhab-Jafari, M. T.; SilDas, S.; Selvaratnam, R.; Melacini, G. *J. Biol. Chem.* **2009**, *284*, 23682−23696.
(40) Akimoto, M.; Selvaratnam, R.; McNicholl, E. T.; Verma, G.; Taylor, S. S.; Melacini, G. *Proc. Natl. Acad. Sci. U. S. A.* **2013**, *110*, 14231−14236.
(41) Das, R.; Mazhab-Jafari, M. T.; Chowdhury, S.; SilDas, S.; Selvaratnam, R.; Melacini, G. *J. Biol. Chem.* **2008**, *283*, 19691−19703.
(42) Huang, L. J. S.; Taylor, S. S. *J. Biol. Chem.* **1998**, *273*, 26739−26746.
(43) Herberg, F. W.; Taylor, S. S.; Dostmann, W. R. G. *Biochemistry* **1996**, *35*, 2934−2942.
(44) Su, Y.; Dostmann, W. R.; Herberg, F. W.; Durick, K.; Xuong, N. H.; Ten Eyck, L.; Taylor, S. S.; Varughese, K. I. *Science* **1995**, *269*, 807−813.
(45) Kim, C.; Cheng, C. Y.; Saldanha, S. A.; Taylor, S. S. *Cell* **2007**, *130*, 1032−1043.
(46) Badireddy, S.; Yunfeng, G.; Ritchie, M.; Akamine, P.; Wu, J.; Kim, C. W.; Taylor, S. S.; Qingsong, L.; Swaminathan, K.; Anand, G. S. *Mol. Cell. Proteomics* **2011**, *10*, M110.004390.
(47) Lorieau, J. L.; Louis, J. M.; Schwieters, C. D.; Bax, A. *Proc. Natl. Acad. Sci. U. S. A.* **2012**, *109*, 19994−19999.
(48) Selvaratnam, R.; Mazhab-Jafari, M. T.; Das, R.; Melacini, G. *PLoS One* **2012**, *7*, 1−9.
(49) Selvaratnam, R.; Vanschouwen, B.; Fogolari, F.; Mazhab-Jafari, M. T.; Das, R.; Melacini, G. *Biophys. J.* **2012**, *102*, 630−639.
(50) Stockman, B. J.; Dalvit, C. *Prog. Nucl. Magn. Reson. Spectrosc.* **2002**, *41*, 187−231.
(51) Boulton, S.; Akimoto, M.; VanSchouwen, B.; Moleschi, K.; Selvaratnam, R.; Giri, R.; Melacini, G. *Biochem. Soc. Trans.* **2014**, *42*, 302−307.
(52) Zhou, L.; Siegelbaum, S. A. *Structure* **2007**, *15*, 655−670.
(53) Akimoto, M.; Zhang, Z.; Boulton, S.; Selvaratnam, R.; Van Schouwen, B.; Gloyd, M.; Accili, E. a.; Lange, O. F.; Melacini, G. *J. Biol. Chem.* **2014**, *289*, 22205−22220.
(54) Lolicato, M.; Nardini, M.; Gazzarrini, S.; Mo̲ller, S.; Bertinetti, D.; Herberg, F. W.; Bolognesi, M.; Martin, H.; Fasolini, M.; Bertrand, J. a.; Arrigoni, C.; Thiel, G.; Moroni, A. *J. Biol. Chem.* **2011**, *286*, 44811−44820.
(55) Rehmann, H.; Wittinghofer, A.; Bos, J. L. *Nat. Rev. Mol. Cell Biol.* **2007**, *8*, 63−73.
(56) Khanh, K. D.; Teigen, K.; Kopperud, R.; Hodneland, E.; Schwede, F.; Christensen, A. E.; Martinez, A.; Døskeland, S. O. *J. Biol. Chem.* **2006**, *281*, 21500−21511.
(57) Kim, C.; Xuong, N.-H.; Taylor, S. S. *Science* **2005**, *307*, 690−696.
(58) Delaglio, F.; Grzesiek, S.; Vuister, G. W.; Zhu, G.; Pfeifer, J.; Bax, A. *J. Biomol. NMR* **1995**, *6*, 277−293.
(59) Goddard, T. D.; Kneller, D. G. *SPARKY 3*; University of California: San Francisco.

DOI: 10.1021/jacs.5b06557
J. Am. Chem. Soc. 2015, 137, 10777−10785